Enhancing Safety and Efficacy of Senolytic Therapies with Advanced Controlled Release Strategies

Vitor Francisco[1,2#], Andreia Marques[1,2,3#], David Sanfeliu-Redondo[4#], Inês Tomé[1,2,5], Susana Rosa[1,2], Joao Pitrez[1,2], Peio Aristu-Zabalza[4], Jordi Gracia-Sancho[4*], Lino Ferreira[1,2,3,6*]

[1]Center for Neuroscience and Cell Biology, University of Coimbra, Coimbra, Portugal

[2]Centre for Innovative Biomedicine and Biotechnology (CiBB), University of Coimbra

[3]Faculty of Medicine, University of Coimbra, 3000-548, Coimbra, Portugal

[4]Liver Vascular Biology Research Group, IDIBAPS Biomedical Research Institute, Hospital Clínic de Barcelona & CIBEREHD, Barcelona, Spain

[5]Faculty of Pharmacy, University of Coimbra, 3000-548, Coimbra, Portugal

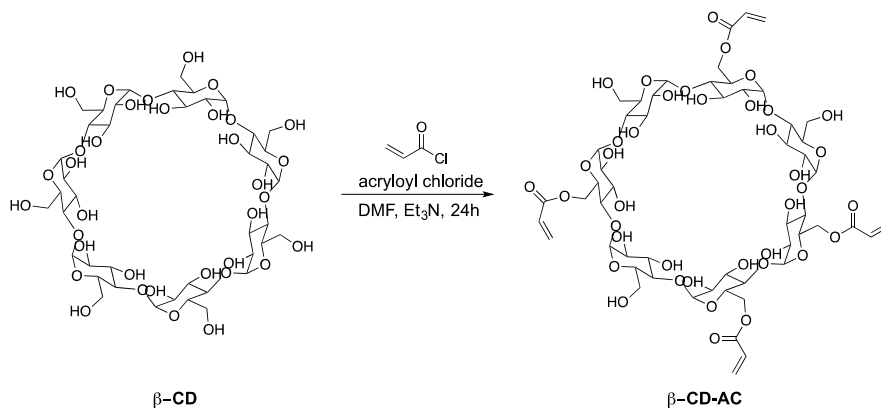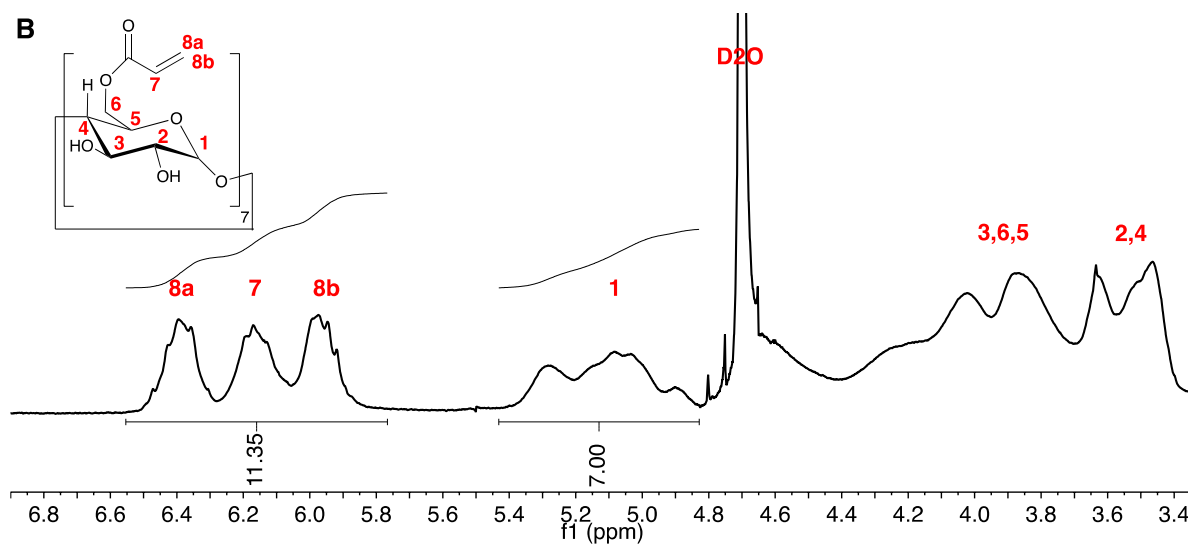[6]Colab4Ageing, Coimbra, Portugal

co-first authors

Corresponding authors:

Email: **Lino.ferreira@uc.pt**

Email: **jgracia@recerca.clinic.cat**

A

β-CD-AC   1-42   P1 to P42

B

Figure S1. Synthesis of β-cyclodextrin polymers. (A) Reaction scheme for the synthesis β-cyclodextrin polymers (P1-P42). (B) Monomers used for the synthesis of the library: acrylated β-cyclodextrin (β-CD-AC) and amines (1-42).

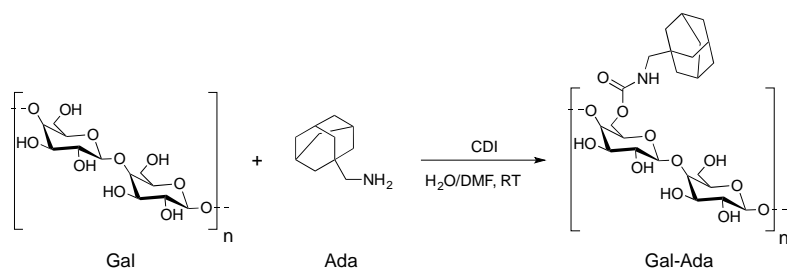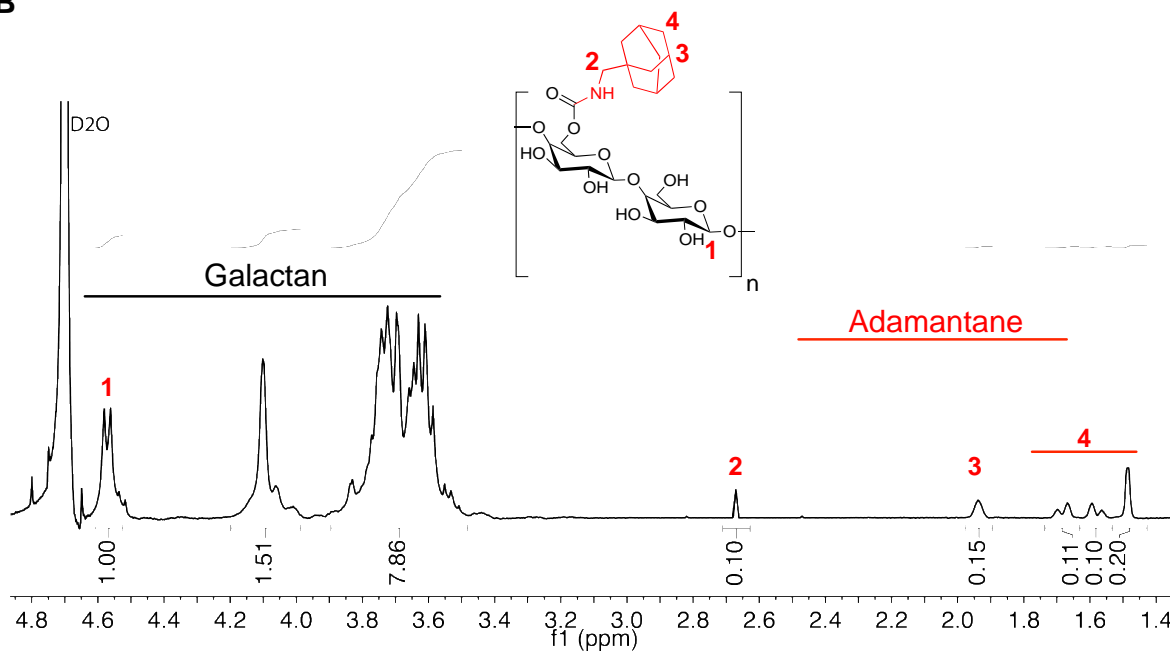**Figure S2.** Modification of β-cyclodextrin. (A) Reaction scheme for the synthesis of acrylated β-cyclodextrin (β-CD-AC). (B) ^{1}H spectrum of β-CD-AC in D_2O. The degree of substitution, number of acrylates per β-cyclodextrin, is 3.8 ± 0.2.
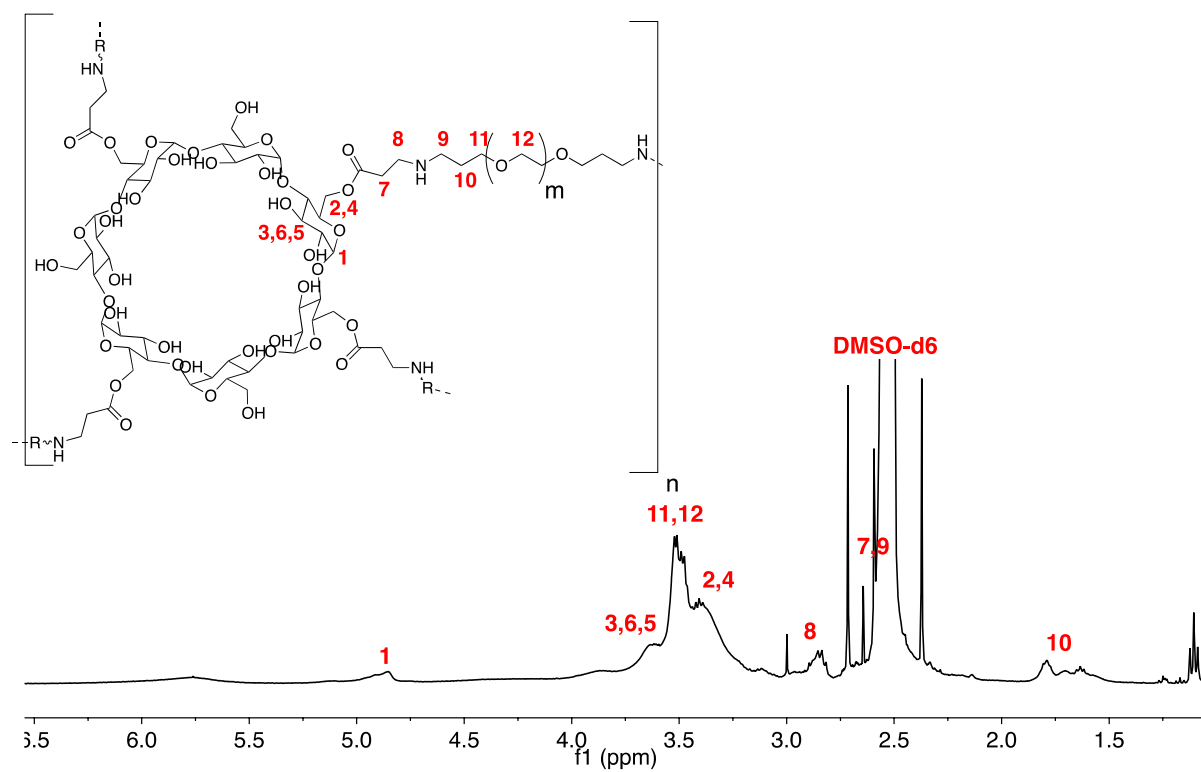
Figure S3. [1]H spectrum of P10 in DMSO-d6. The absence of acrylate protons between 6.0 to 6.5 ppm indicates high amine capping polymers.
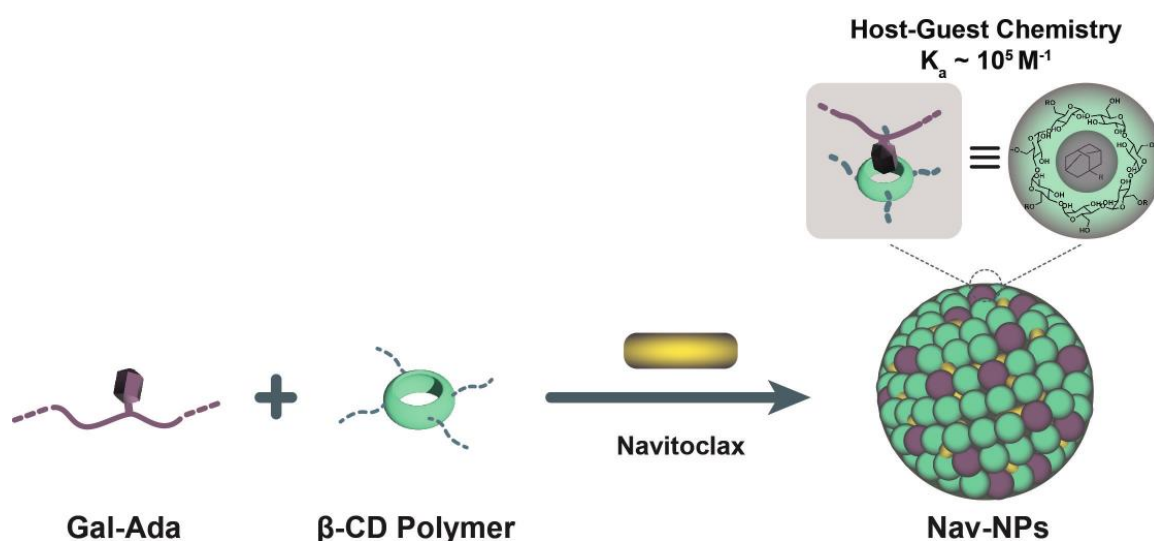
Figure S4. Synthesis of galactan-adamantane guest polymer. (A) Reaction scheme for the preparation of adamantane containing galactan (Gal-Ada). (B) ^{1}H-NMR spectrum of Gal-Ada in D_2O. The degree of substitution of adamantane on the galactan polymer was determined by the ratio between proton 1 (galactan) and proton 3 (adamantane).
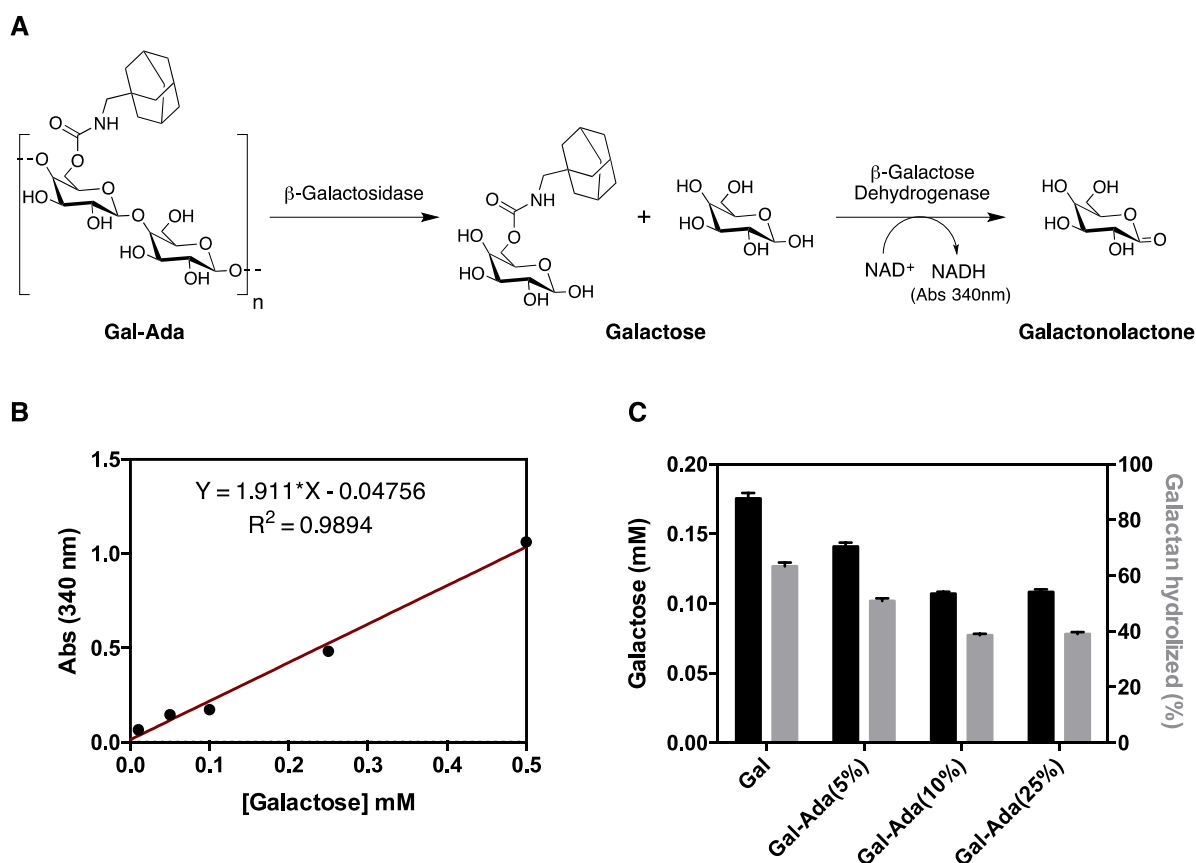
Figure S5. Enzymatic cleavage of adamantane-modified galactan with different degree of substitution (DS). (A) Reaction scheme of Gal-Ada degradation by enzyme β-galactosidase and galactose quantification by the reduction of NAD⁺ to NADH at 340 nm by β-galactose dehydrogenase (Gal-DH assay). (B) Calibration curve for the determination of D-galactose. (C) Quantification of galactose and galactan hydrolysed from galactan with different DS (5%, 10% and 25%) by Gal-DH assay, after cleavage by β-galactosidase (*Aspergillus oryzae*). Results are expressed as Means ± SEM (*n* = 3).

A

Host-Guest Chemistry
$K_a \sim 10^5 \, M^{-1}$

Gal-Ada + β-CD Polymer → Navitoclax → Nav-NPs

B

C

NP10	NP efficiency formation (%)	NPs count decrease (%)
Gal-Ada_5%	15.5 ± 2.4	86.5 ± 5.4
Gal-Ada_10%	25.4 ± 3.5	73.4 ± 6.5
Gal-Ada_25%	34.5 ± 6.2	14.5 ± 7.2

Figure S6. Optimization of NP formation and disassembly. (A) Schematic representation of the NP assembly through host-guest interactions between β-cyclodextrin polymers (P1 to P42) and adamantane-modified galactan (Gal-Ada) to encapsulate the senolytic drug Navitoclax. (B) Photograph of different solutions showing the successful formation of NPs: 1) aqueous solution of Gal-Ada, 2) mixture of β-cyclodextrin polymer randomly selected (P10) with Gal-Ada (host-guest ratio of 2:1) and 3) aqueous solution of polymer P10. (C) Responsiveness of the assembled NPs with different synthesized Gal-Ada to the enzyme β-Galactosidase. The NPs (1 mg/mL) were formed with the selected polymer and incubated with β-Galactosidase (*Aspergillus oryzae,* 20 units) for 4 h at 37 °C. The NPs count decrease were determined by DLS by the ratio between the number of NPs before addition of the enzyme and the number of NPs determined 4 h after enzyme addition. Results are expressed as Means ± SEM (*n* = 3).

A

B

C
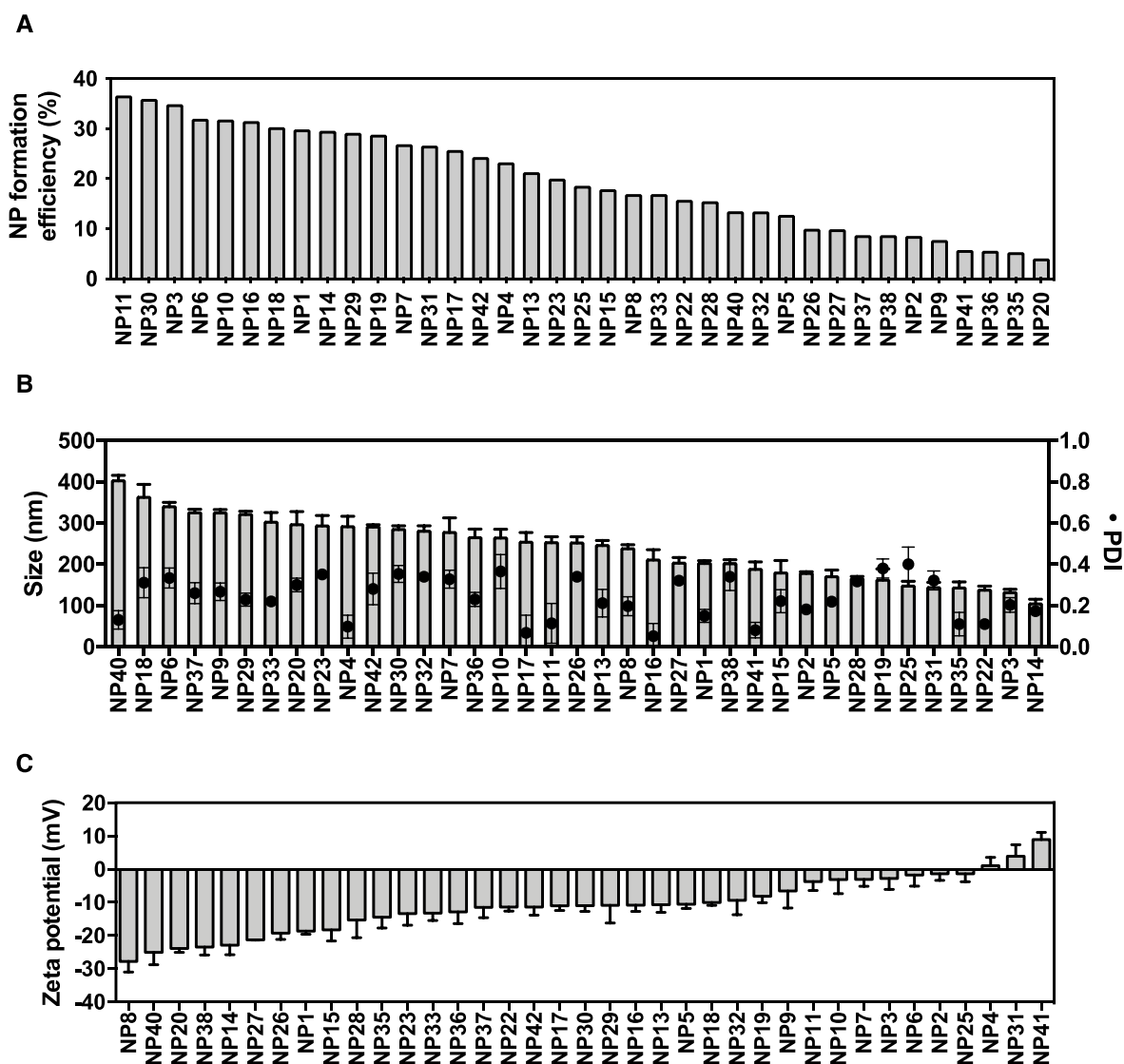
Figure S7. Physicochemical properties of the NP library. (A) NP formation efficiency (%). The data was calculated by the ratio between the weight of NPs after purification and the initial theoretical weight of the polymers. (B) NP size (left axis) and NP polydispersity index (PDI) (right axis). (C) Zeta potential of the NPs measured by DLS. Results are expressed as Means ± SEM ($n = 3$).

A

B
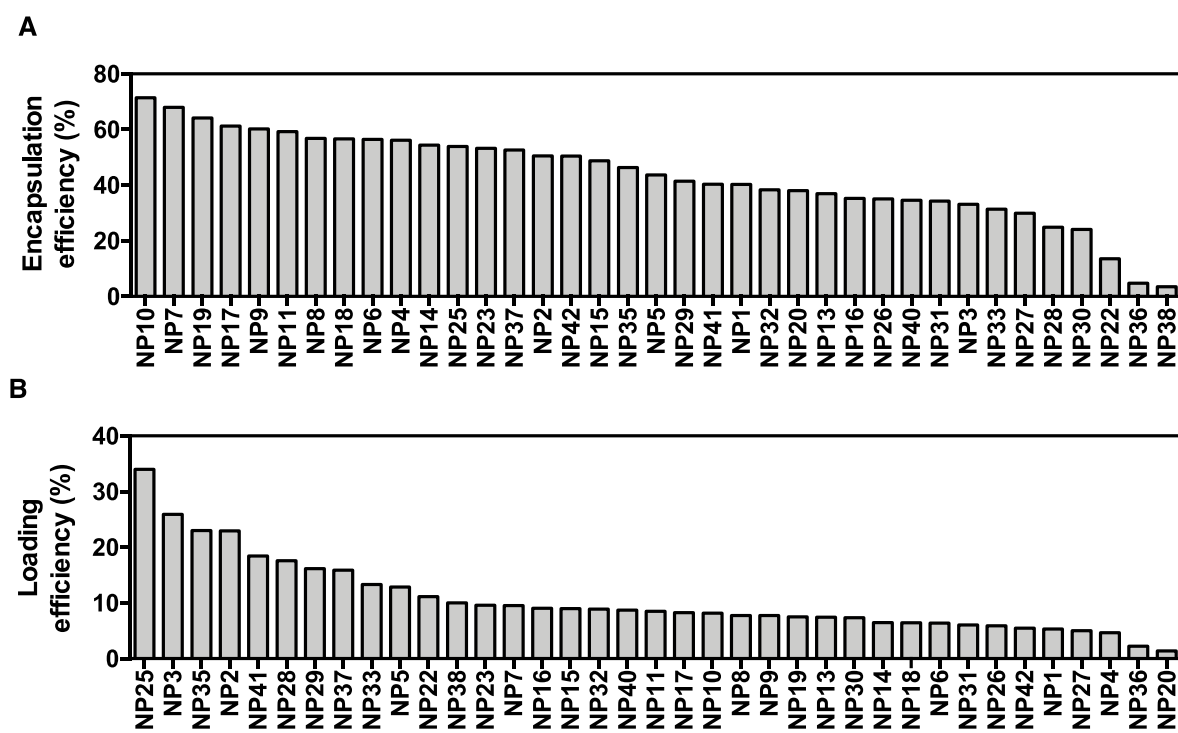
Figure S8. Encapsulation efficiency (A) and loading efficiency (B) of Navitoclax by the NPs.
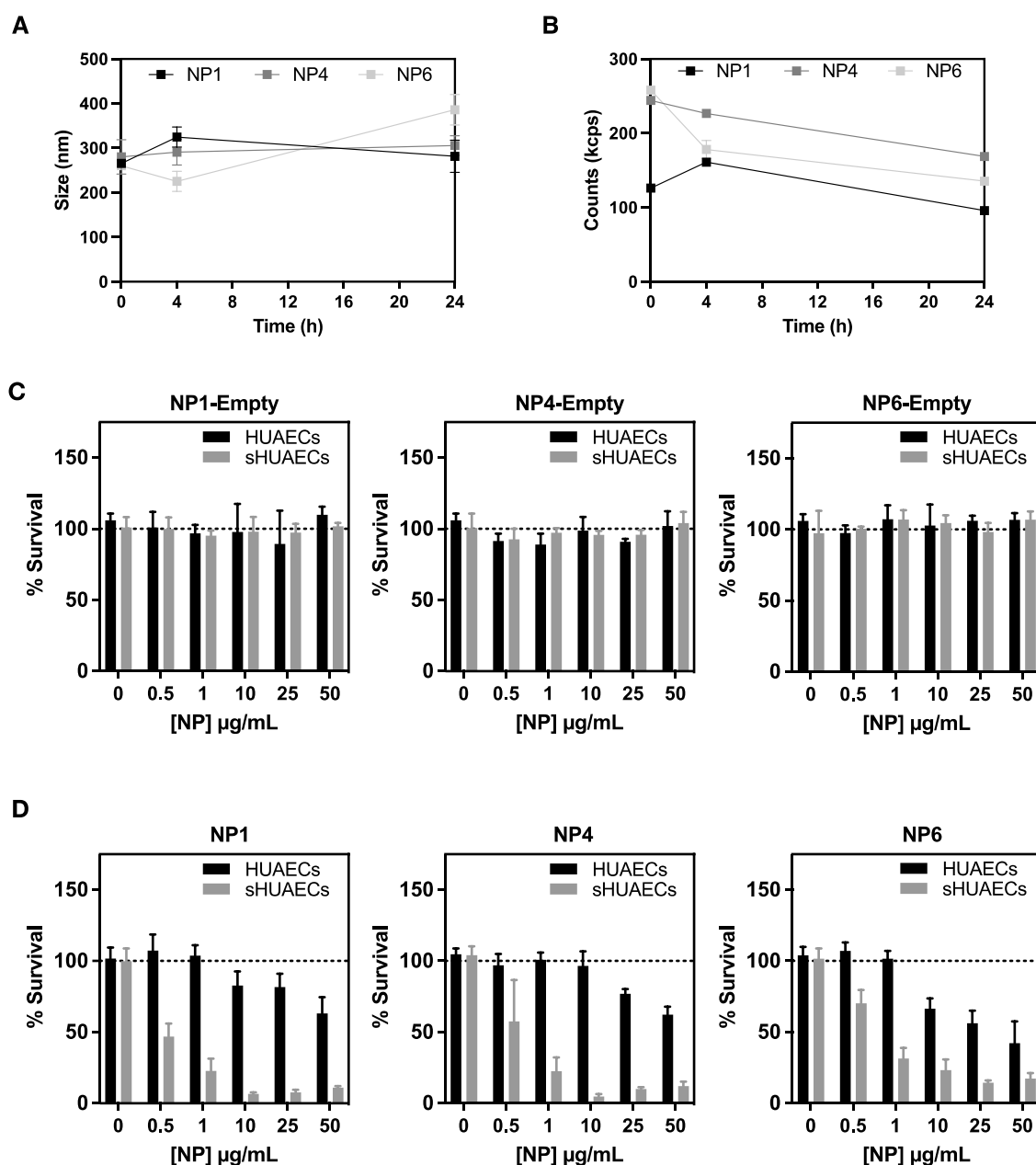
Figure S9. Stability and cytotoxicity of NPs. (A) DLS analysis of size and (B) NP counts overtime of randomly selected NPs, NP1, NP4 and NP6 (50 µg/mL) in EGM-2 medium with FBS (10%). (C, D) Cell survival after exposure to NP1, NP4 and NP6, without (C) and with (D) Navitoclax. Cells were incubated at different concentration for 4 h, washed and after 48 h cell nuclei were stained with Hoechst H33342 and propidium iodide to assess cell survival. Cell survival was calculated as the % of viable cell from the total count of nuclei. Results are presented as Mean ± SEM (n = 3).
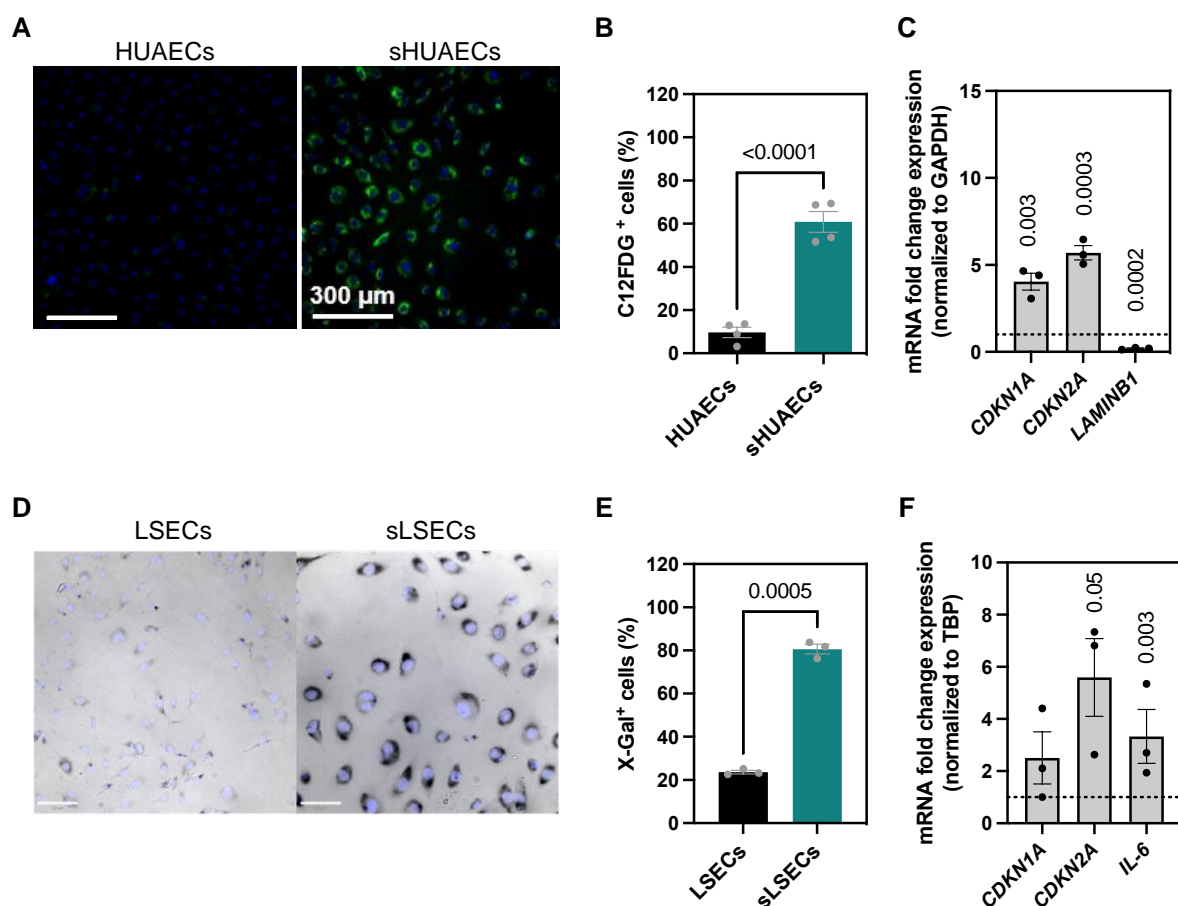
Figure S10. Characterization of the senescence phenotype in sHUAECs and sLSECs. (A, B) Representative image (A) and quantification (B) of C12FDG+ cells in sHUAECs characterised 7 days after irradiation with 10 Gy gamma-irradiation. HUAECs stained with Hoechst (blue) and fluorescent substrate $C_{12}FDG$ (green). Scale bar is 300 µm. (C) Expression levels of p21, p16 and lamin B1 genes assessed by qRT-PCR analysis in sHUAECs at day 7 days post-irradiation. Data was normalised to housekeeping gene *GAPDH*. Dashed line indicates mRNA expression in proliferative cells. Values on top of the columns are *p* values (calculated between sHUAECs and HUAECs). (D, E) Representative image (D) and quantification (E) of X-Gal+ cells of LSECs characterised 10 days after irradiation with 10 Gy gamma-irradiation. Scale bar is 100 µm. (F) Expression levels of p21 and p16 and IL-6 genes assessed by real-time PCR analysis. Data was normalised to housekeeping gene *TBP*. Dashed line indicates mRNA expression in proliferative cells. Results are presented as Means ± SEM (*n* = 3). In B, C, E and F, *p* values were determined by a Student's t test.
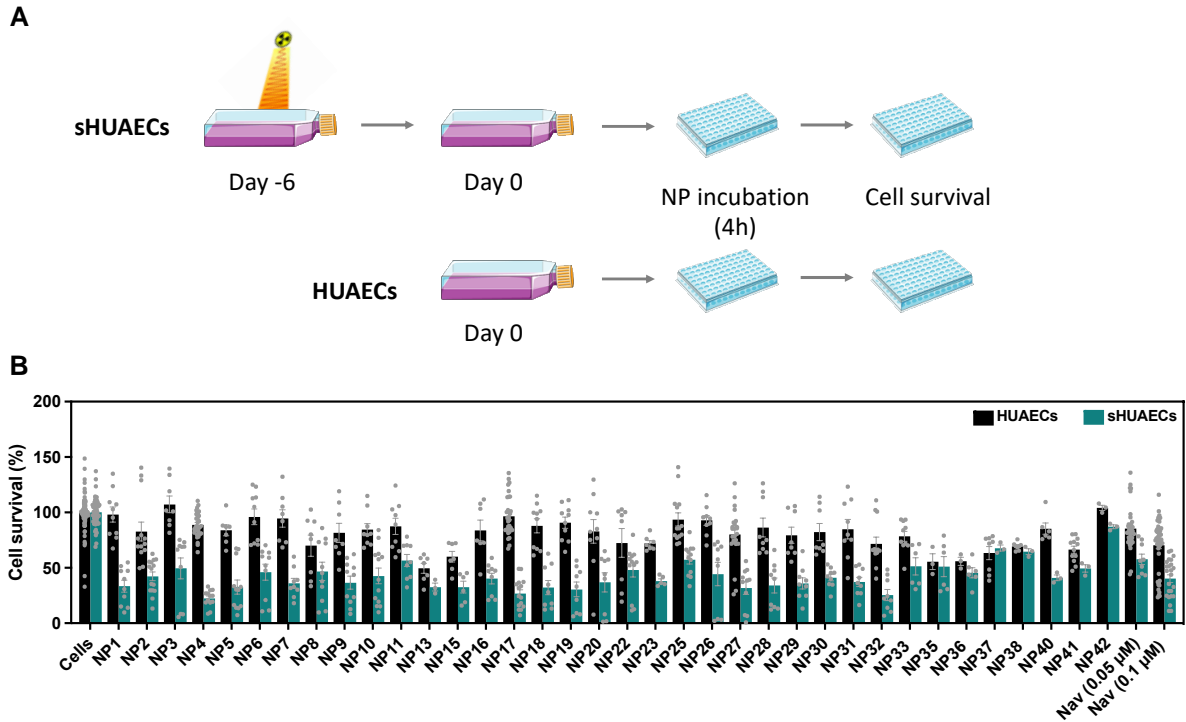
Figure S11. High-throughput screening of the NP library against HUAECs and sHUAECs. (A) Scheme for high-throughput screening of the NP library. (B) HUAECS and sHUAECs were incubated with the NPs (1 μg/mL) for 4 h, washed 3x with DMEM to remove non-internalized NPs and cell survival assessed at 48 h. Control groups are HUAECs and sHUAECs with no treatment or exposed to soluble Nav (0.05 μM or 0.1 μM). Results are expressed as Mean ± SEM ($n \geq 3$; ≥ 36 microscope fields each). Each dot in the graph represents an independent experiment.
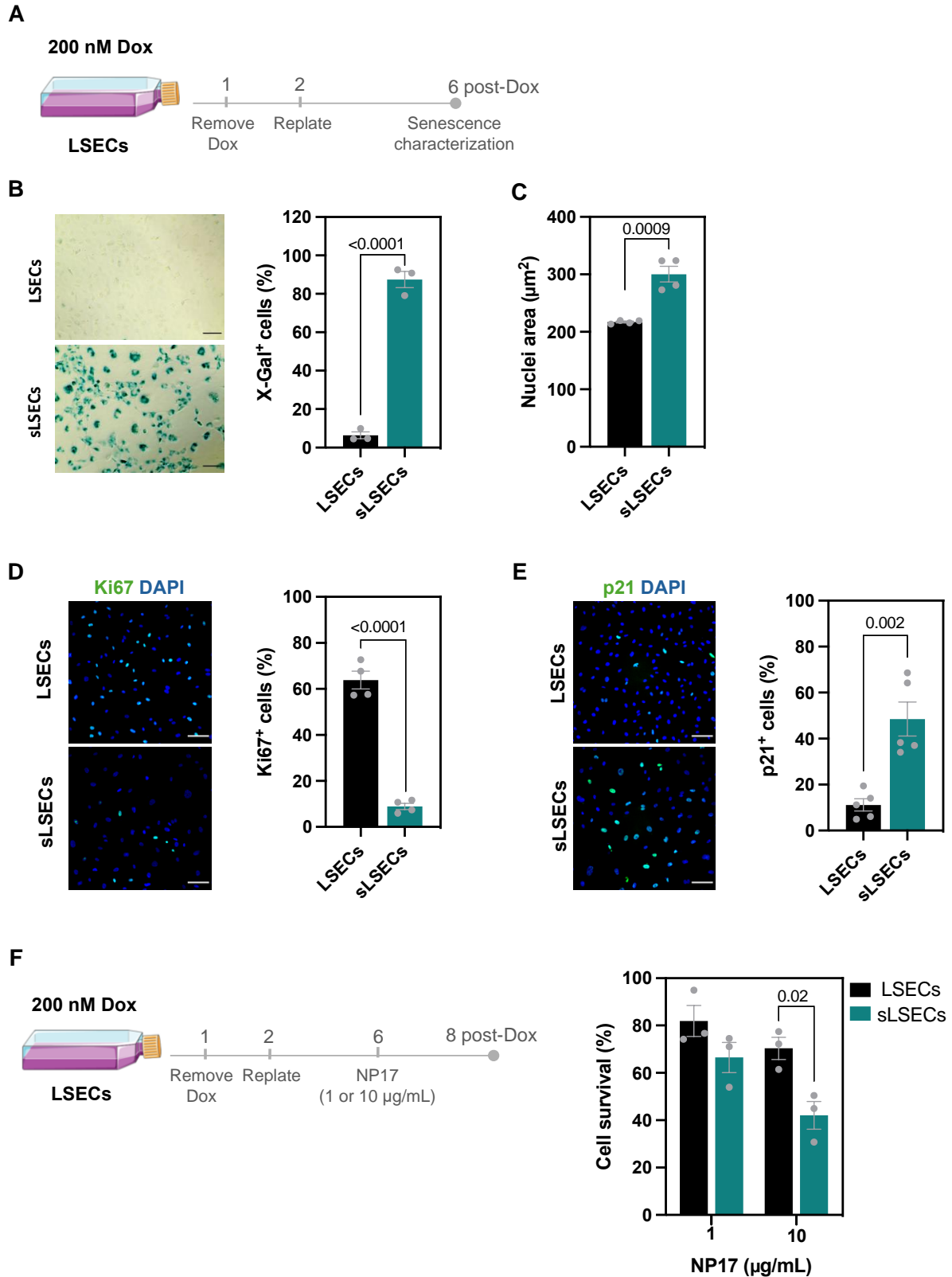
Figure S12. LSECs senescence induced by doxorubicin and bioactivity of NP17. (A) LSECs were exposed to 200 nM of Doxorubicin (Dox) for 24 h and then replated in 96-multiwells. At day 6 post-Dox, cells were characterized for different senescent markers. (B) Representative image and quantification of X-Gal⁺ cells. Magnification is 20x and scale bars are 100 μm. (C)

Nuclei area. In B and C, results are expressed as Mean ± SEM ($n \geq 3$; 10 fields/image). (D, E) Representative images and quantification of Ki67 (D) and (E) p21 expression in sLSECs (day 6 post-Dox). Magnification is 20x and scale bars are 100 µm. (F) At day 6 post-Dox, LSECs were exposed to NP17 at different concentrations and cell viability was evaluated after 48 h using Hoechst and Propidium Iodide staining. Results are normalized to cells exposed only with cell media. Results are expressed as Mean ± SEM ($n \geq 3$). Each dot in the graph represents an independent experiment. Statistical analyses were performed by a Student's t-test.
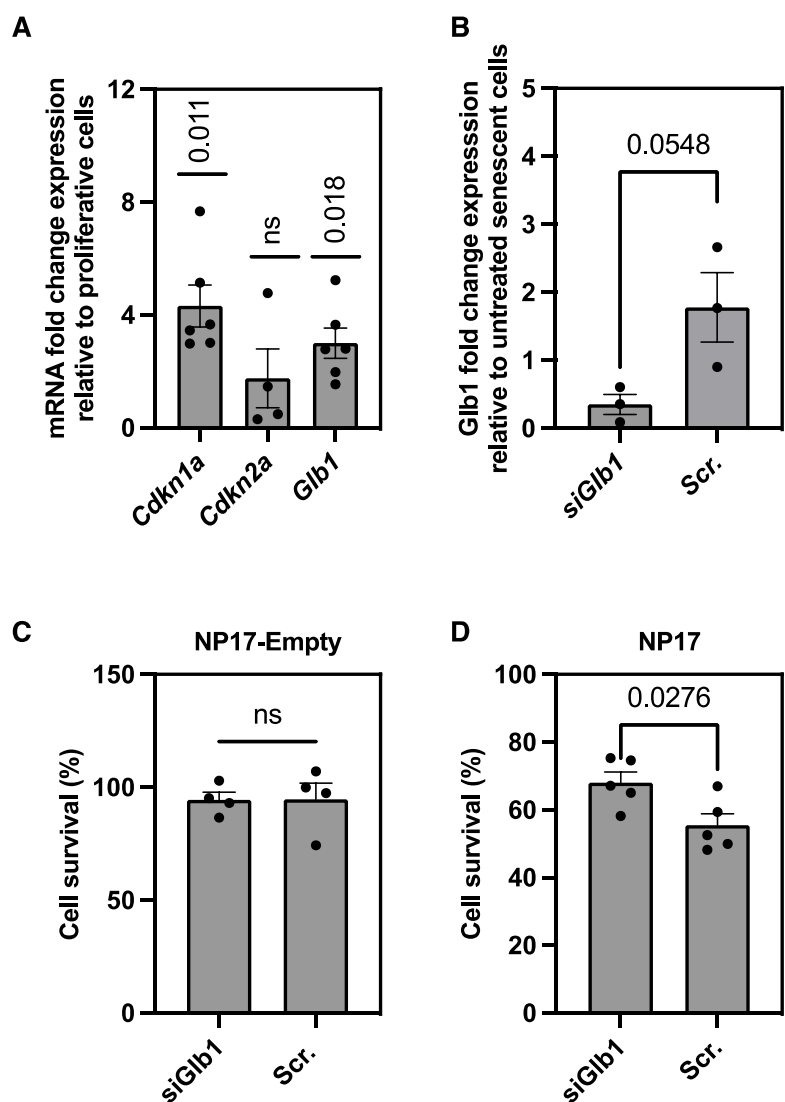
Figure S13. Senolytic activity of NP17 in senescent cells before and after *Glb1* knockdown by a siRNA. (A) Fold change in mRNA expression of *Cdkn1a*, *Cdkn2a* and *Glb1* of gamma-irradiation induced A549 cells. (B) Glb1 fold change gene expression in senescent A549 cells 48 h post-transfection with siRNA targeting Glb1 mRNA (siGlb1) or scramble siRNA (Scr). The results have been normalized to untreated senescent cells. (C) Percentage of cell survival upon 48 h NP17-Empty (C) or NP17 (D) (1 µg/mL) treatment of senescent A549 previously transfected with siRNA against Glb1 or scramble. In A, B, C and D, results are expressed as Mean ± SEM ($n \geq 3$). Each dot in the graph represents an independent experiment. In C and D, a total of 30 images were analysed per experiment. Statistical analyses were performed by a Student's t-test.

A	**B**	**C**
NP4	**NP17**	**NP16**
K (min⁻¹) 0.02021	**K (min⁻¹)** 0.01553	**K (min⁻¹)** 0.00329
Half-Time (min) 34.29	**Half-Time (min)** 44.64	**Half-Time (min)** 210.3
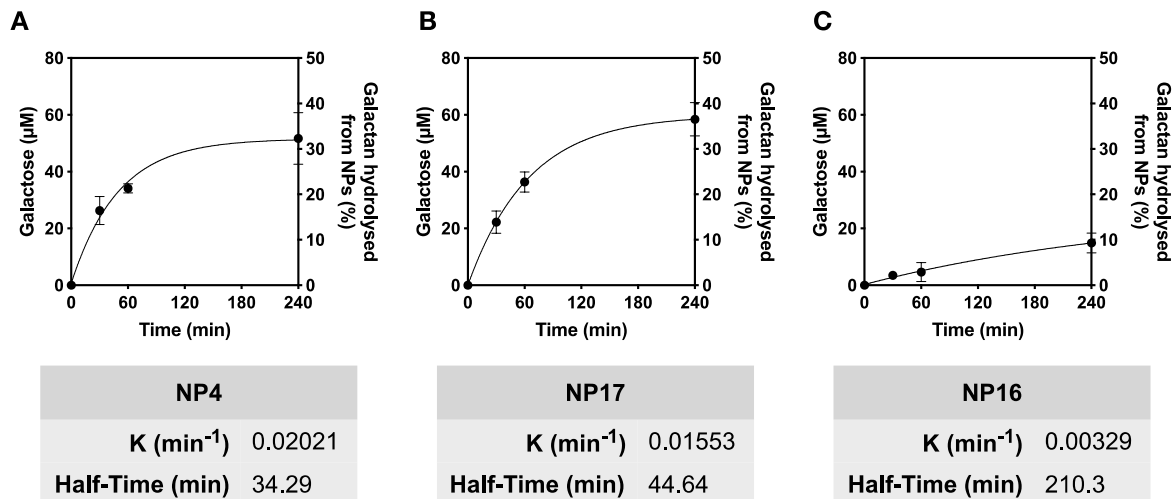
Figure S14. NP degradation kinetics. A suspension of Nav-loaded NPs (1 mg/mL) was treated with 20 units of β-galactosidase. At specific time points, a volume was removed from the sample, centrifuged and the supernatant diluted in β-galactose dehydrogenase. The galactose concentration was determined by the Gal-DH assay (see Materials and Methods). (A) Quantification of galactose concentration released from the hit (NP4 and NP17) (B) and non-hit formulation (NP16) (C), upon enzymatic degradation by β-galactosidase. The black line shows the fitting to an one-phase association curve to describe the pseudo-first order association kinetics of the interaction between the galactan and β-galactosidase using Prism software. Results are expressed as Means ± SEM (n = 3).
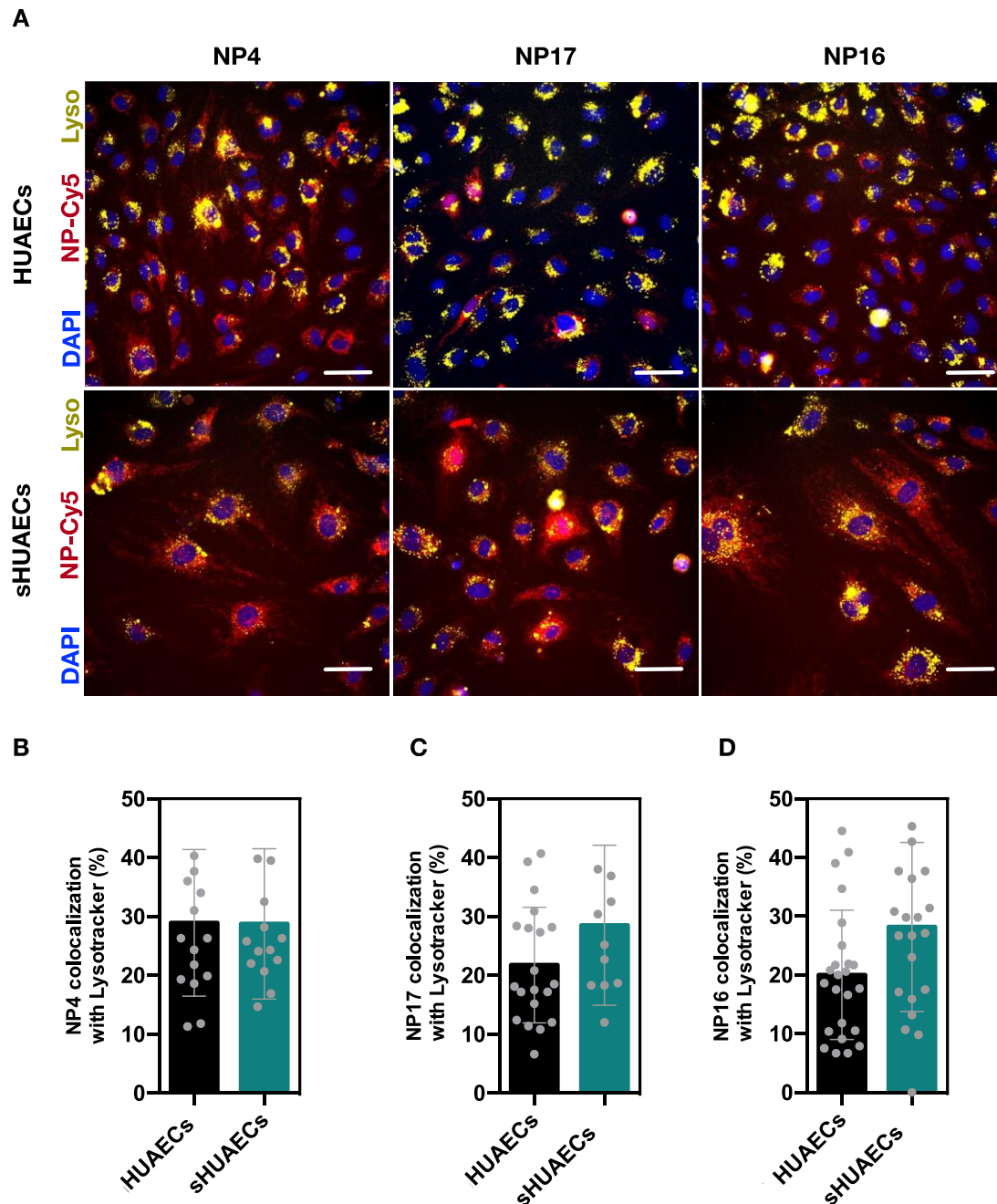
Figure S15. Cellular internalization of the NPs. (A) Representative fluorescence microscopy images showing the co-localization of NP4, NP17 and NP16 formulation labelled with Cy5 with endolysosomal compartment (stained with Lysotracker). Co-localization of NPs with endolysosomes is relatively easy to monitor by the yellow foci´s. Scale bar is 50 µm. (B) Quantification of the co-localization of hit (NP4 and NP17) (C) and non-hit formulations (NP16) (D) with endolysosomes in HUAECs at 4 h post incubation with NPs (1 µg/mL). Co-localization between NP17 and endolysosomal compartment expressed as the Manders' overlap coefficient quantified by ImageJ analyses. The results are expressed as Means ± SEM ($n = 4$, 3 to 6 microscope fields each). The dots in the graph corresponds to each microscopic field.
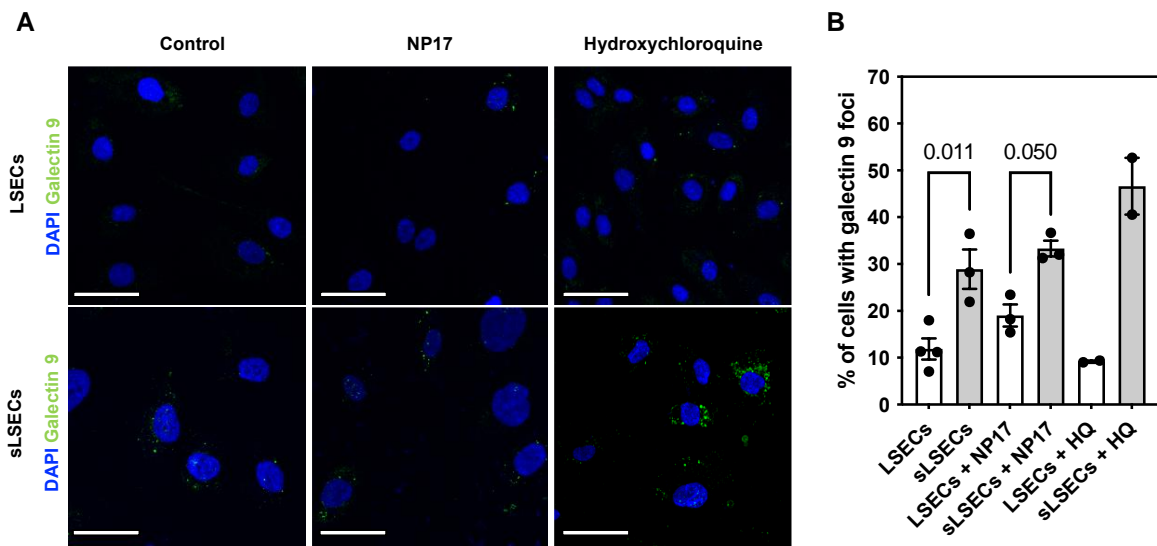
Figure S16. NP endolysosomal escape evaluated by galectin-9 staining. (A) Representative images of LSECs and senescent LSECs (sLSECs) stained for galectin-9 after treatment with NP17 (10 μg/mL) or hydrochloroquine (100 μm) for 4 h. Scale bar is 50 μm. (B) Quantification of the percentage of LSECs with at least one galectin-9 foci per cell. Results are expressed as Mean ± SEM ($n \geq 2$; a total of 4-10 fields (20-30 nuclei/field) and 4-10 fields (10-20 nuclei/field) were analyzed from proliferative and senescent cells, respectively). Each dot in the graph represent an independent experiment. Statistical analysis was assessed by one-way ANOVA followed by Tukey's multiple comparisons test.
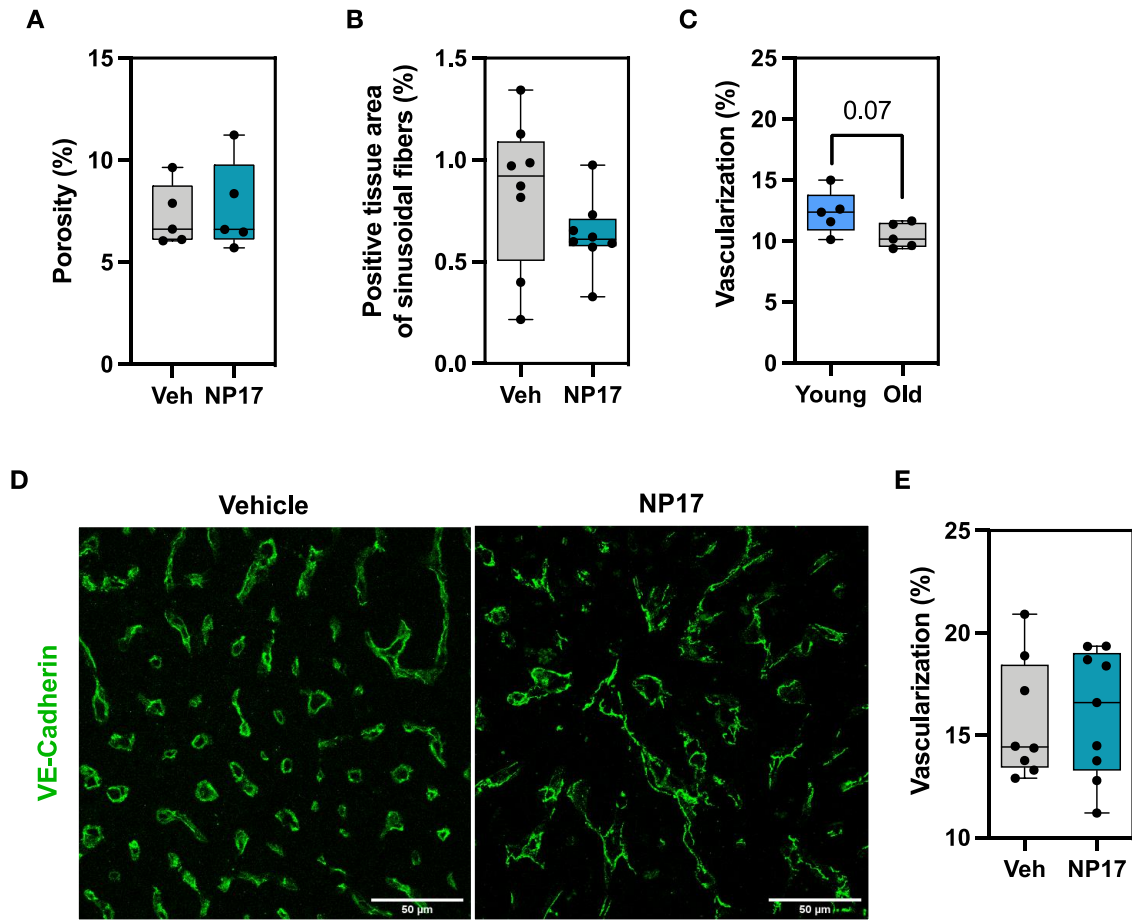
Figure S17. Impact of NP17 in the liver vascular network. (A) Quantification of the porosity of LSECs (n = 5/group). Six randomly selected blocks from each animal were mounted onto stubs and coated with gold. Ten images were acquired per animal. (B) Quantification of LSEC fibers (n = 8/group). (C) Percentage of intrahepatic neovascularization of young vs old rats. (D) Immunofluorescence staining of rat liver cryosections for VE-cadherin. Vascularization of sinusoidal cells corresponds to the % of vessels (in μm^2) in a determined ROI. At least 10 ROIs were identified per sample. Scale bar is 50 μm. (E) Percentage of intrahepatic neovascularization (n = 8/group). Each dot in the graphs represents an independent experiment. In A, B, C and E, values are presented as box and whiskers plots with min to max values.
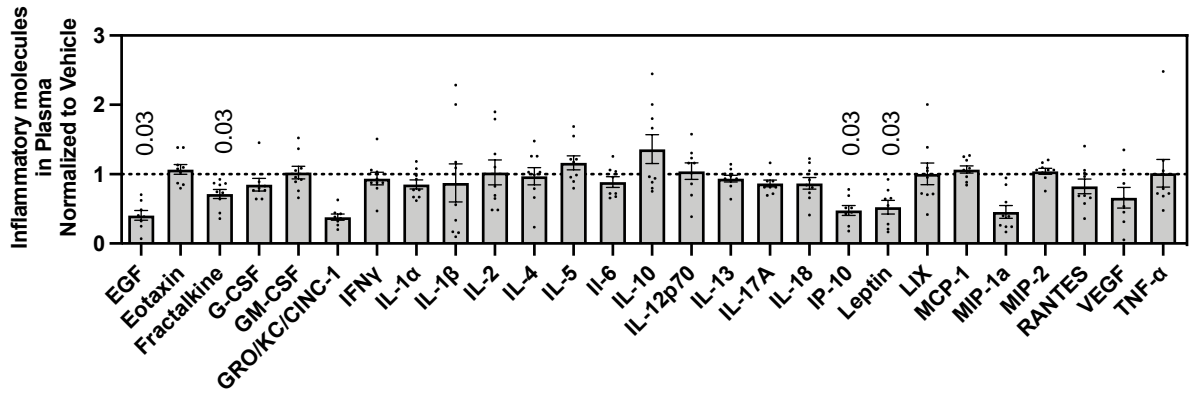
Figure S18. Profiling of inflammatory molecules in plasma of aged rats treated with NP17 (normalized to vehicle levels; $n \geq 7$/group). Aged male Wistar rats (20 months old) were administered through the penile vein with NP17 or vehicle. The treatments were administered for 2 weeks (4 doses *per* week), with a 1-week of interval in between. For the injection of the NPs or the vehicle, rats were anesthetized with isoflurane. Animals were allowed to recover for an additional 4 weeks without any manipulation. The results are expressed as Mean ± SEM. *p* values above data refer to the comparison of NP17 *versus* vehicle.

Table S1. Senolytic index (SI) of compounds from in vitro studies. The senolytic index (SI) is defined as the ratio between the IC_{50} of proliferative (P) cells and the IC_{50} of senescent (S) cells.
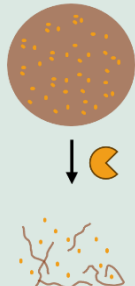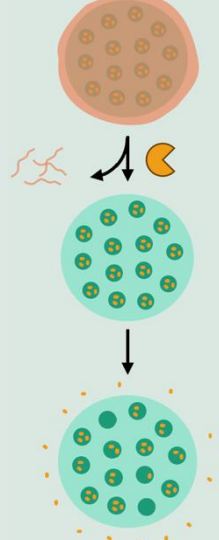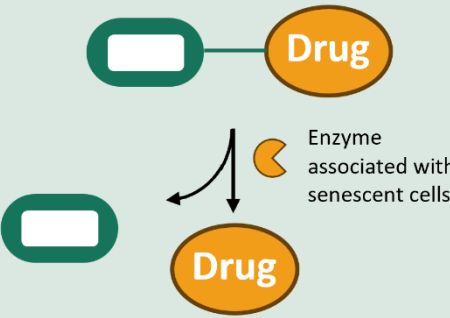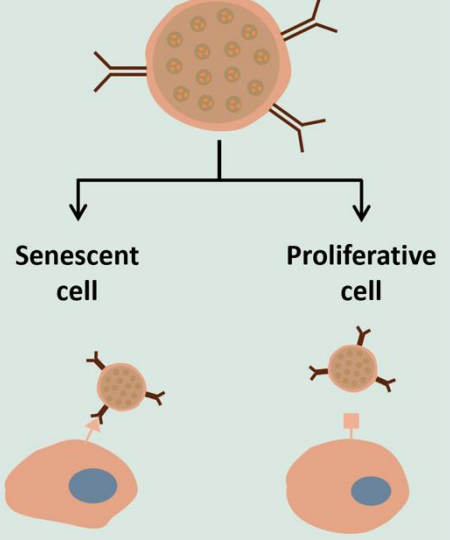
Senolytic	Delivery method	Cell model	IC_{50} of proliferative (P) and senescent (S) (μM)*	SI ($IC_{50}P/IC_{50}S$)	References
Digitoxin	Soluble	IMR90 ER:RAS	H>10.000; S=0.0375#	>266	[1]
Navitoclax	NP	WI-38	H=61.620; S=0.4300	143.0	[2]
Bufalin	Soluble	IMR90 ER:RAS	H=1.272; S=0.0105#	121.0	[1]
Navitoclax	Prodrug	SK-Mel-103	H=0.125; S=0.0016	78.5	[3]
Ouabain	Soluble	IMR90 ER:RAS	H=1.422; S=0.0296#	48.0	[1]
Navitoclax	Prodrug	A549	H=9.758; S=0.2750	35.5	[3]
PZ15227	PROTAC	WI-38	H>10.000; S=0.2900#	34.5	[4]
Navitoclax	Soluble	WI-38	H=9.030; S=0.3200	28.0	[2]
Navitoclax	Soluble	SK-Mel-103	H=0.028; S=0.0011	25.7	[3]
SSK1	Prodrug	NBFs	H>1.000; S=0.0400a	25.0	[5]
Digoxin	Soluble	IMR90 ER:RAS	H=1.655; S=0.0720#	23.0	[1]
Navitoclax	Soluble	A549	H=1.926; S=0.1220	15.9	[3]
Periplocin	Soluble	IMR90 ER:RAS	H=0.300; S=0.0240a	12.3	[6]
FOXO4-DRI	Soluble	IMR90	H=55.000; S=4.7000a	11.7	[7]
Ginkgetin	Soluble	IMR90 ER:RAS	H=26.000; S=2.6000a	8.9	[6]
17-DMAG	Soluble	MEFs	H=0.069; S=0.0080#	8.6	[8]
SSK1	Prodrug	Lung FBs	H>1.000; S=0.1500a	6.7	[5]
Oleandrin	Soluble	IMR90 ER:RAS	H=0.085; S=0.0140a	5.8	[6]
JHB75B	Prodrug	IMR90 ER:RAS	H=7.113; S=1.2780a	5.6	[9]
SSK1	Prodrug	HUVECs	H=0.100; S=0.0300a	3.3	[5]
D+Q	Soluble	HUVECs	H=0.200; S=0.0600a	3.0	[10]
Quercetin	Soluble	HUVECs	H=20.000; S=10.000a	2.0	[10]
Fisetin	Soluble	HUVECs	H>60.000; S=30.0000a	>2	[11]

Notes: IMR90 ER:RAS – Human Primary Fibroblasts with an ER:RAS inducible construct; WI-38 - Wistar Institute-38 human diploid fibroblast cells; SK-Mel-103 - Sloan Kettering Melanoma-103 cells; A549 - Adenocarcinomic human alveolar basal epithelial cells; NBFs – New born dermal fibroblasts; MEFs – Mouse embryonic fibroblasts; Lung FBs – Adult mouse lung fibroblasts; HUVECs – Human umbilical vein endothelial cells. *IC_{50} (or #EC_{50}) of proliferative and senescent cells values were either collected directly from the literature or estimated (a) based on the reported graphs.

Table S2. Morphometry data and hemodynamic assessment 4 weeks after treatment. Values are Mean ± SEM (n=8). Data followed normality and statistical significance was evaluated by ANOVA test with Tukey's post hoc correction. *Veh *vs.* Nav, †Veh *vs.* NP17, ¥Nav *vs.* NP17. No differences were found between Nav and NP17 rats. BW, body weight; SMABF, superior mesenteric arterial blood flow; ALT, alanine transaminase; AST, aspartate transaminase; Portal blood flow index and Intrahepatic resistance index are normalized by liver weight (g).

	Vehicle	Navitoclax	NP17	*p*-value
Morphometry				
Body weight (g)	582.00 ± 17.78	597.13 ± 25.59	569.75 ± 25.56	
Brain weight / BW	0.38 ± 0.02	0.39 ± 0.02	0.41 ± 0.02	
Liver weight / BW	2.37 ± 0.08	2.19 ± 0.12	2.39 ± 0.04	
Spleen weight / BW	0.18 ± 0.01	0.17 ± 0.01	0.18 ± 0.02	
Lung's weight / BW	0.30 ± 0.01	0.33 ± 0.03	0.31 ± 0.01	
Kidney's weight / BW	0.55 ± 0.02	0.54 ± 0.01	0.54 ± 0.02	
Pancreas weight / BW	0.19 ± 0.02	0.16 ± 0.01	0.17 ± 0.02	
Quadriceps weight / BW	1.10 ± 0.05	1.17 ± 0.11	0.85 ± 0.06	
Hemodynamic analysis				
Mean arterial pressure (mmHg)	84.17 ± 1.97	86.48 ± 3.52	87.21 ± 2.92	
Heart rate (beats/min)	313.98 ± 10.42	296.15 ± 6.67	312.39 ± 14.54	
Temperature (ºC)	37.03 ± 0.16	37.02 ± 0.11	36.97 ± 0.14	
Portal pressure (mmHg)	9.33 ± 0.25	9.13 ± 0.26	8.67 ± 0.20	
Portal blood flow (mL/min)	22.26 ± 1.31	21.96 ± 1.90	23.36 ± 1.54	
Portal blood flow index	1.68 ± 0.13	1.74 ± 0.18	1.73 ± 0.12	
Intrahepatic resistance	0.43 ± 0.04	0.43 ± 0.03	0.38 ± 0.03	
Intrahepatic resistance index	5.83 ± 0.56	5.61 ± 0.57	5.20 ± 0.45	
SMABF (mL/min)	18.96 ± 2.69	14.35 ± 1.47	17.17 ± 1.64	
Liver biochemistry				
ALT (U/L)	155.50 ± 27.94	80.38 ± 8.69*	115.22 ± 16.74	*0.03
AST (U/L)	208.38 ± 30.46	141.50 ± 21.07	216.44 ± 36.70	
Albumin (g/L)	26.88 ± 0.48	27.25 ± 0.73	28.13 ± 0.30	

Table S3. Senotherapeutic delivery strategies.

	1. NPs that release their cargo more specifically in senescent cells		2. Prodrugs	3. Senescent cell targeted NPs
Senotherapeutic release	High and rapid Our approach	Slow and limited 12,13	Not applicable 3,5,9	Slow and limited 14
Carrier degradability	Degradable	Non-degradable (potential cytotoxic effects)	Degradable	Non-degradable (potential cytotoxic effects)
Senolytic index	High (up to 1425)	Moderate (up to 143)	Moderate (up to 78)	Low
Liver accumulation	High	High	No evidence	High

Table S4. Examples of drugs targeting specific pathways involved in liver fibrosis on clinical trials (completed, recruiting or active). Comparison of our nanoformulation (NP17) with other drugs regarding fibrosis reduction in liver fibrosis animal models[a].

Therapy	Animal model	Fibrosis level (at vs bt) (mean ± SEM)	Fibrosis reduction (%)	Dosage (mg/kg/day)	References
NP17	Wistar rats (Aged-20 months old)	2.55 ± 0.1 vs 3.13 ± 0.30	18.5	0.2	
Liraglutide	Wistar rats (Cirrhosis)	9.25 ± 1.8 vs 12.01 ± 1.85	23.0	0.5	[15]
BMS-986036	C57BL/6J mice (NASH)	3.27 ± 0.2 vs 4.1 ± 0.17	20.2	0.6	[16]
Tropifexor	C57BL/6J mice (NASH)	0.55 ± 0.1 vs 1.0 ± 0.2	45.0	0.9	[17]
Aramchol	C57BL/6J mice (NASH)	2.3 ± 0.1 vs 5.3 ± 1.3[#]	55.0	5.0	[18]
Cenicriviroc	Sprague-Dawley rats (TAA-induced fibrosis)	15.0 ± 5.0 vs 22.0 ± 6.5 (SD)[#]	35.7	30.0	[19]
Simtuzumab	C57BL/6J mice (TAA-induced fibrosis)	2.7 ± 0.1 vs 3.2 ± 0.2[#]	53.4	30.0	[20]
Nitazoxanide	C57BL/6J mice (CCl4-induced fibrosis)	3.0 ± 2.0 vs 9.0 ± 4.0 (SD)[#]	66.7	100.0	[21]
Lanifibranor	Sprague-Dawley rats (Cirrhosis)	14.0 ± 4.0 vs 17.0 ± 3.0[#]	32.0	100.0	[22]

Notes: NASH - Nonalcoholic steatohepatitis; TAA - Thioacetamide; CCl4 – Carbon tetrachloride; at vs at – after treatment vs before treatment; [#]Estimated values from the reported graph.

[a] In this study, we examined the reduction of liver fibrosis in aged Wistar rats, comparing our findings with animal models of nonalcoholic steatohepatitis (NASH)-induced fibrosis and cirrhosis. While the effectiveness of antifibrotic drugs has been extensively documented in models of NASH and cirrhosis, there is a notable deficiency in research focused on their application to age-related fibrosis[23,24]. This is because fibrosis in aged animal models poses unique challenges due to the combined effects of cellular senescence and systemic aging[25]. Our findings suggest that the formulation can effectively target fibrosis in aged livers, even at lower doses compared to those typically required for antifibrotic drugs in clinical trials.

Table S5. Information of chemical name, CAS number and vendor of the monomers used to synthesize the library of β-cyclodextrin-based polymers.

Monomer	Chemical Name IUPAC	CAS	Vendor
1	Ethylenediamine	107-15-3	Merck
2	1,4-Diaminobutan	110-60-1	Aldrich
3	1,6-Diaminohexan	124-09-4	Alfa Aesar
4	Diethylenetriamine	111-40-0	Alfa Aesar
5	Triethylenetetraamine	112-24-3	Acros Organics
6	Pentaethylenehexamine	4067-16-7	Aldrich
7	3,3'-Diamino-N-methyldipropylamine	105-83-9	Aldrich
8	1,2-Diaminocyclohexane	694-83-7	Aldrich
9	1,8-Diamino-3,6-dioxaoctane	929-59-9	Acros Organics
10	1,13-Diamino-4,7,10-trioxatridecane	4246-51-9	Aldrich
11	1,4-Bis(aminopropyl)piperazine	7209-38-3	Aldrich
12	1,4-Phenylenedimethanamine	539-48-0	Merck
13	1,5-Diaminonaphthalene	2243-62-1	Aldrich
14	4,4'-methylenedianiline	101-77-9	Aldrich
15	1,3-Phenylenediamine	108-45-2	TCI Chemicals
16	1,3-Diaminopropane	109-76-2	TCI Chemicals
17	2,2-Dimethyl-1,3-propanediamine	7328-91-8	TCI Chemicals
18	1,3-Diaminopentane	589-37-7	TCI Chemicals
19	2,2'-Diamino-N-methyldiethylamine	4097-88-5	TCI Chemicals
20	Agmatine sulfate	2482-00-0	TCI Chemicals
21	1,4-Bis(aminomethyl)cyclohexane	2579-20-6	TCI Chemicals
22	4,4'-Methylenebis(cyclohexylamine)	1761-71-3	Aldrich
23	4,4'-Diaminobenzanilide	785-30-8	Aldrich
24	DL-Lysine	70-53-1	Aldrich
25	3-Amino-1-propanol	156-87-6	Aldrich
26	4-Amino-1-butanol	13325-10-5	Aldrich
27	5-Amino-1-pentanol	2508-29-4	Sigma Aldrich
28	6-Amino-1-hexanol	4048-33-3	Alfa Aesar
29	1-(3-Aminopropyl)pyrrolidine	23159-07-1	Alfa Aesar
30	1-(3-Aminopropyl)imidazole	5036-48-6	Aldrich
31	1-(3-Aminopropyl)-4-methylpiperazine	224-954-4	Alfa Aesar
32	Histamine	51-45-6	Sigma Aldrich
33	2-(2-Aminoethoxy)ethanol	929-06-6	Sigma Aldrich
34	3-methoxypropan-1-amine	5332.73-0	Sigma Aldrich
35	(+-)-3-Amino-1,2-propanediol	616-30-08	Sigma Aldrich
36	2-Amino-1,3-propanediol	534-03-2	Sigma Aldrich
37	4-Aminobutyraldehyde dimethyl acetal	19060-15-2	Alfa Aesar
38	4-Hydrazinobenzenesulfonic acid	98-71-5	TCI Chemicals
39	Sulfanilic Acid	121-57-3	TCI Chemicals
40	1,3 - Phenylenediamine-4-sulfonic Acid	88-63-1	TCI Chemicals
41	Tris(2-aminoethyl)amine	4097-89-6	Sigma Aldrich
42	2-Methoxyethylamine	109-85-3	Sigma Aldrich

Table S6. List of pre-designed mouse primer pairs from Sigma-Aldrich.

Gene	Sample	Primer Sequence (5' to 3')
Gapdh	In vitro - HUAECs and A549	FW: AGCCACATCGCTCAGACACC
		RV: GTACTCAGCGCCAGCATCG
Tbp	In vitro - LSECs	FW: GCCAAGAGTGAAGAACAG
		RV: GAAGTCCAAGAACTTAGCTG
Cdkn1a	In vitro - HUAECs, A549 and LSECs	FW: CAGCATGACAGATTTCTACC
		RV: CAGGGTATGTACATGAGGAG
Cdkn2a	In vitro - HUAECs, A549 and LSECs	FW: AGCATGGAGCCTTCG
		RV: ATCATGACCTGGATCGG
Il6	In vitro - LSECs	FW: GCAGAAAAGGCAAAGAAT
		RV: CTACATTTGCCGAAGAGC
Glb1	In vitro - A549	FW: GACAGTACCAGTTTTCTGAG
		RV: ATAGACTCTTTCTCTAGCAGC

Table S7. Antibodies used for immunofluorescence.

Antibody	Reference and manufacturer	Specie	Triton (v/v)	Dilution
Primary Antibodies				
HMGB1	ab18256, Abcam	Rabbit	1 %	1:250
VWF	A0082, Dako	Rabbit	0.1 %	1:200
VE-Cadherin	AF1002, R&D systems	Goat	-	1:100
Galactin-9	348902, BioLegend	Mouse	-	1:100
Secondary Antibodies				
AlexaFluor™ 448 donkey anti-goat IgG IgG (H+L)	A11055, Invitrogen			1:500
AlexaFluor 555 goat anti-rabbit IgG	A21428, Invitrogen			1:500

References:

1   Guerrero, A. *et al.* Cardiac glycosides are broad-spectrum senolytics. *Nat Metab* **1**, 1074-1088 (2019). https://doi.org:10.1038/s42255-019-0122-z

2   Escriche-Navarro, B., Garrido, E., Sancenon, F., Garcia-Fernandez, A. & Martinez-Manez, R. A navitoclax-loaded nanodevice targeting matrix metalloproteinase-3 for the selective elimination of senescent cells. *Acta Biomater* **176**, 405-416 (2024). https://doi.org:10.1016/j.actbio.2024.01.002

3   Gonzalez-Gualda, E. *et al.* Galacto-conjugation of Navitoclax as an efficient strategy to increase senolytic specificity and reduce platelet toxicity. *Aging Cell* **19**, e13142 (2020). https://doi.org:10.1111/acel.13142

4   He, Y. *et al.* Using proteolysis-targeting chimera technology to reduce navitoclax platelet toxicity and improve its senolytic activity. *Nat Commun* **11**, 1996 (2020). https://doi.org:10.1038/s41467-020-15838-0

5   Cai, Y. *et al.* Elimination of senescent cells by beta-galactosidase-targeted prodrug attenuates inflammation and restores physical function in aged mice. *Cell Res* **30**, 574-589 (2020). https://doi.org:10.1038/s41422-020-0314-9

6   Smer-Barreto, V. *et al.* Discovery of senolytics using machine learning. *Nat Commun* **14**, 3445 (2023). https://doi.org:10.1038/s41467-023-39120-1

7   Baar, M. P. *et al.* Targeted Apoptosis of Senescent Cells Restores Tissue Homeostasis in Response to Chemotoxicity and Aging. *Cell* **169**, 132-147 e116 (2017). https://doi.org:10.1016/j.cell.2017.02.031

8   Fuhrmann-Stroissnigg, H. *et al.* Identification of HSP90 inhibitors as a novel class of senolytics. *Nat Commun* **8**, 422 (2017). https://doi.org:10.1038/s41467-017-00314-z

9   Guerrero, A. *et al.* Galactose-modified duocarmycin prodrugs as senolytics. *Aging Cell* **19**, e13133 (2020). https://doi.org:10.1111/acel.13133

10   Zhu, Y. *et al.* The Achilles' heel of senescent cells: from transcriptome to senolytic drugs. *Aging Cell* **14**, 644-658 (2015). https://doi.org:10.1111/acel.12344

11   Zhu, Y. *et al.* New agents that target senescent cells: the flavone, fisetin, and the BCL-X(L) inhibitors, A1331852 and A1155463. *Aging (Albany NY)* **9**, 955-963 (2017). https://doi.org:10.18632/aging.101202

12   Agostini, A. *et al.* Targeted cargo delivery in senescent cells using capped mesoporous silica nanoparticles. *Angew Chem Int Ed Engl* **51**, 10556-10560 (2012). https://doi.org:10.1002/anie.201204663

13   Munoz-Espin, D. *et al.* A versatile drug delivery system targeting senescent cells. *EMBO Mol Med* **10** (2018). https://doi.org:10.15252/emmm.201809355

14   Thapa, R. K. *et al.* Progressive slowdown/prevention of cellular senescence by CD9-targeted delivery of rapamycin using lactose-wrapped calcium carbonate nanoparticles. *Sci Rep* **7**, 43299 (2017). https://doi.org:10.1038/srep43299

15   de Mesquita, F. C. *et al.* Liraglutide improves liver microvascular dysfunction in cirrhosis: Evidence from translational studies. *Sci Rep* **7**, 3255 (2017). https://doi.org:10.1038/s41598-017-02866-y

16   Tang, H. *et al.* Evaluation of a PEGylated Fibroblast Growth Factor 21 Variant Using Novel Preclinical Magnetic Resonance Imaging and Magnetic Resonance Elastography in a Mouse Model of Nonalcoholic Steatohepatitis. *J Magn Reson Imaging* **56**, 712-724 (2022). https://doi.org:10.1002/jmri.28077

17   Hernandez, E. D. *et al.* Tropifexor-Mediated Abrogation of Steatohepatitis and Fibrosis Is Associated With the Antioxidative Gene Expression Profile in Rodents. *Hepatol Commun* **3**, 1085-1097 (2019). https://doi.org:10.1002/hep4.1368

18   Iruarrizaga-Lejarreta, M. *et al.* Role of Aramchol in steatohepatitis and fibrosis in mice. *Hepatol Commun* **1**, 911-927 (2017). https://doi.org:10.1002/hep4.1107

19   Lefebvre, E. *et al.* Antifibrotic Effects of the Dual CCR2/CCR5 Antagonist Cenicriviroc in Animal Models of Liver and Kidney Fibrosis. *PLoS One* **11**, e0158156 (2016). https://doi.org:10.1371/journal.pone.0158156

20   Ikenaga, N. *et al.* Selective targeting of lysyl oxidase-like 2 (LOXL2) suppresses hepatic fibrosis progression and accelerates its reversal. *Gut* **66**, 1697-1708 (2017). https://doi.org:10.1136/gutjnl-2016-312473

21   Liu, K. X. *et al.* The antiprotozoal drug nitazoxanide improves experimental liver fibrosis in mice. *Biochem Pharmacol* **224**, 116205 (2024). https://doi.org:10.1016/j.bcp.2024.116205

22   Boyer-Diaz, Z. *et al.* Pan-PPAR agonist lanifibranor improves portal hypertension and hepatic fibrosis in experimental advanced chronic liver disease. *J Hepatol* **74**, 1188-1199 (2021). https://doi.org:10.1016/j.jhep.2020.11.045

23   Tewari, D. *et al.* Fenugreek (Trigonella foenum-graecum L.) Seeds Dietary Supplementation Regulates Liver Antioxidant Defense Systems in Aging Mice. *Nutrients* **12** (2020). https://doi.org:10.3390/nu12092552

24   Tsukahara, Y. *et al.* Administration of Glutaredoxin-1 Attenuates Liver Fibrosis Caused by Aging and Non-Alcoholic Steatohepatitis. *Antioxidants (Basel)* **11** (2022). https://doi.org:10.3390/antiox11050867

25   Delire, B. *et al.* Aging enhances liver fibrotic response in mice through hampering extracellular matrix remodeling. *Aging (Albany NY)* **9**, 98-113 (2016). https://doi.org:10.18632/aging.101124